PERGAMON

International Journal of Heat and Mass Transfer 45 (2002) 5117–5132

International Journal of HEAT and MASS TRANSFER

www.elsevier.com/locate/ijhmt

Interaction between discrete heat sources in horizontal natural convection enclosures

Qi-Hong Deng [a,*], Guang-Fa Tang [a], Yuguo Li [b], Man Yeong Ha [c]

[a] College of Civil Engineering, Hunan University, Changsha, Hunan 410082, China
[b] Department of Mechanical Engineering, The University of Hong Kong, Hong Kong, China
[c] School of Mechanical Engineering, Pusan National University, Pusan 609-735, South Korea

Received 7 March 2002; received in revised form 14 June 2002

Abstract

Steady natural convection induced by multiple discrete heat sources (DHSs) in two-dimensional horizontal enclosures is numerically investigated. A general combined temperature scale method is first implemented to identify the DHSs of both external and internal types. An associated concept of thermal strength is then introduced in terms of the unified heat transfer characteristics of DHSs to analyze the interaction among them. Four different calculation cases are detailed analyzed, and main attention has been focused on the effects of the Rayleigh number (Ra), the thermal strength (Π), and the separation distance (W^*) on the interaction between DHSs. Computational results demonstrated that the combined temperature scale method and the unified heat transfer characteristics analysis are convenient and efficient to evaluate the complex interaction between DHSs and its effects on the fluid flow and heat transfer structures in horizontal natural convection enclosures.

1. Introduction

Natural convection heat transfer in rectangular enclosures continues to be an active research area, due to its significance for both fundamental interests and engineering applications [1–3]. There are two elementary classes of natural convection flows in enclosures, namely, those in vertical enclosures with two differentially heated vertical walls and those in horizontal enclosures with differentially heated horizontal walls. With the ultimate aim to simulate realistic flows found in engineering applications, considerable attention has been given to natural convection due to discrete heat sources (DHSs) [4–17]. The resulting fluid flow and heat transfer structures are governed by the interaction between DHSs and hence become more complex than that induced by a single heat source [18,19].

So far almost all studies on natural convection with multiple DHSs have been limited to vertical cases and can be grouped into three classes: natural convection with DHSs along vertical plates [4–8]; natural convection with DHSs in vertical enclosures [9–13]; natural convection with both external and internal heat sources in vertical enclosures [14–17]. However, the buoyancy induced natural convection by DHSs in horizontal enclosures is of at least equal importance and found in various engineering applications, such as cooling of electronic components and air-conditioning of buildings with chilled ceilings. From the viewpoint of the flow pattern and heat transfer characteristics, natural convection with DHSs in horizontal enclosures can be much more complex than that occurring in vertical enclosures or along vertical plates. For natural convection with DHSs distributing on the same vertical surface, one prevailing upward circulating flow structure is formed by the buoyancy effect, and therefore the upper heat source is significantly affected by the thermal plume induced by the lower heat source, but the lower is hardly affected by the upper. Compared to the passive effect of vertical case, the interaction between the DHSs in horizontal enclosure, however, would be more active because they have to "struggle" seriously for their subsistence within

* Corresponding author. Fax: +86-731-882-1005.
E-mail address: dengqh2001@sina.com (Q.-H. Deng).

0017-9310/02/$ - see front matter
PII: S0017-9310(02)00221-1

Nomenclature

A	area of the volumetric heat source
A_r	aspect ratio of the enclosure
g	gravitational acceleration
H, L	height and length of the enclosure
k	thermal conductivity
l	length of the surface heat source
$\mathbf{n}$	unit normal vector
N	number of discrete heat sources
Nu	local Nusselt number
$\overline{Nu}$	average Nusselt number
P	dimensionless pressure
Pr	Prandtl number
q''	heat flux of surface heat source
q'''	heat flux of volumetric heat source
R	contribution ratio
Ra	Rayleigh number
S	source term
T	temperature
ΔT	characteristic temperature scale
u, v	velocity components in x, y directions
U, V	dimensionless velocities in X, Y directions
W	distance between discrete heat sources
x, y	Cartesian coordinates
X, Y	dimensionless coordinates

Greek symbols

α	thermal diffusivity of the fluid
β	coefficient of thermal expansion
θ	dimensionless temperature
v	kinematic viscosity of the fluid
ρ	density of the fluid
ω	weight coefficient
Π	strength of the heat source
ψ	streamfunction

Subscripts

c	cold wall
h	hot wall
m	maximum
f	fluid
s	solid
F	isoflux heat source
T	isothermal heat source
V	volumetric heat source

Superscript

$*$	parameter ratio

the limited space. The resulting characteristics of fluid flow and heat transfer are quite interesting and deserve a detailed investigation. The lack of research on this subject has motivated the present work.

To study the interaction between DHSs, the common approach adopted in all above-mentioned literatures is to choose the temperature difference induced by one heat source as the characteristic temperature scale, and then the other heat sources are identified by their temperature difference ratios to the characteristic scale. The method is here referred to as the single temperature scale method. Although being widely used, the method has some disadvantages. First, it is not a physical but numerical approach, for it is unable to reveal the physically inherent interactions between DHSs and also inefficient to describe the characteristics of fluid flow and heat transfer. Second, it is not complete from the mathematical point of view, for it does not work when the characteristic heat source strength approaches zero. Third, it is inconvenient to examine the interaction between any two heat sources and/or among all heat sources, which is however inevitable or important when more than two DHSs exist, because their relative strengths are all based on the referenced scale. Alternatively in the former work [20], we proposed a combined temperature scale method for analyzing natural convection with discrete wall heat sources. The method was found efficient to describe the multiple DHSs and hence their interactions. The present study extends the method to analyze natural convection with DHSs in a general sense with both external wall heat sources and internal volumetric heat sources.

The main objective of the present paper is to establish an efficient approach to evaluate natural convection in horizontal enclosures induced by multiple DHSs. A general combined temperature scale is first set up to non-dimensionalize the governing equations and the boundary conditions (BCs), then the effects of DHSs can be distinguished by their corresponding contribution ratios. Next, unified heat transfer characteristics of DHSs are analyzed in terms of energy conservation across the enclosures, based on which the thermal strengths are defined to determine their roles in the interaction. Finally, the interactions between DHSs and their effects on the fluid and thermal structures are systematically investigated for four different cases. Note that the proposed method is in fact general and suitable for other convection problems with multiple DHSs.

2. Model formulation

2.1. Physical model

The physical model and coordinate system of the problem under consideration are illustrated schemati-

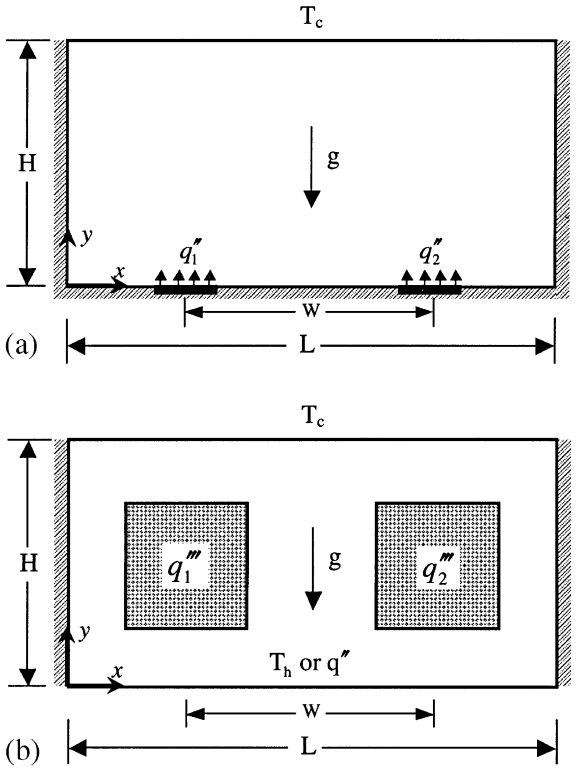

Fig. 1. A schematical model for natural convection in horizontal enclosures with DHSs: (a) two isoflux sources located on the floor and (b) one isothermal or isoflux floor and two inner-volumetric sources.

cally in Fig. 1. They are two-dimensional rectangular cavities of height H and length L, filled with a Newtonian fluid such as air and water. The vertical side walls are all insulated and the top ceiling is maintained at a low temperature T_c. The discretely heated sources are distributed in two manners: Fig. 1(a) shows that two flush-mounted heat sources, respectively with lengths l_1 and l_2 and fluxes q_1'' and q_2'', are positioned on the adiabatic floor with a separation distance W; Fig. 1(b) shows the case that the bottom floor are kept at either a high temperature T_h or a uniform heat flux q'', and meanwhile two volumetric heat sources, respectively with areas A_1 and A_2 and heat-generating rates q_1''' and q_2''', are located inside with a separation distance W. The gravitational acceleration acts in the negative vertical direction.

According to the physical configurations, the interaction between the DHSs in present analysis is divided into four cases: Case 1—two isoflux heat sources (IFHSs) on the floor; Case 2—one isothermal heat source (ITHS) on the floor and two inner-volumetric heat sources (IVHSs); Case 3—one IFHS on the floor ($q'' \neq 0$) and two IVHSs; Case 4—two IVHSs with floor adiabatic ($q'' = 0$). The first case is shown in Fig. 1(a) and the other cases in Fig. 1(b).

2.2. Governing equations

The analysis is based on the two-dimensional steady continuity, momentum, and energy equations in a dimensionless form. All the fluid properties are assumed constant except that the density in the buoyancy term following the Boussinesq approximation. The conservative governing equations for fluids are as follows:

Continuity equation

$$\frac{\partial U}{\partial X}+\frac{\partial V}{\partial Y}=0 \tag{1}$$

Momentum equations

$$\frac{\partial}{\partial X}(UU)+\frac{\partial}{\partial Y}(VU)=-\frac{\partial P}{\partial X}+Pr\nabla^2 U \tag{2}$$

$$\frac{\partial}{\partial X}(UV)+\frac{\partial}{\partial Y}(VV)=-\frac{\partial P}{\partial Y}+Pr\nabla^2 V+RaPr\theta \tag{3}$$

Energy equation

$$\frac{\partial}{\partial X}(U\theta)+\frac{\partial}{\partial Y}(V\theta)=\nabla^2\theta \tag{4}$$

For the volumetric heat-generating conducting solid body, the energy equation becomes

$$\frac{\partial}{\partial X}\left(k_i^*\frac{\partial\theta}{\partial X}\right)+\frac{\partial}{\partial Y}\left(k_i^*\frac{\partial\theta}{\partial Y}\right)+S_i=0 \tag{5}$$

where the source term $S_i=q_i'''H^2/k_f\Delta T$, and relative conductivity $k^*=k_s/k_f$.

The governing equations are non-dimensionalized using scales H, α/H and ΔT for length, velocity and temperature respectively, where the characteristic temperature scale ΔT is defined in detail later. Accordingly, the dimensionless variables are $(X,Y)=(x,y)/H$, $(U,V)=(u,v)/\alpha/H$, $P=p/\rho(\alpha/H)^2$, $\theta=(T-T_c)/\Delta T$, and two dimensionless parameters are defined as $Pr=\nu/\alpha$, $Ra=g\beta\Delta TH^3/\nu\alpha$.

2.3. Combined temperature scale

To identify different heat sources, one should define the characteristic temperature scale, ΔT. If there is a single heat source, the scale can be uniquely determined as follows:

$$\begin{aligned}&\Delta T=T_h-T_c \quad \text{for ITHS;}\\ &\Delta T=q''H/k_f \quad \text{for IFHS;}\\ &\Delta T=q'''H^2/k_f \quad \text{for IVHS}\end{aligned} \tag{6}$$

When more than one heat source is involved, the traditional single temperature scale method is inefficient

and hence the combined temperature scale method is adopted here. The philosophy of the method is that the overall heat transfer could be considered as the combined contribution from all the DHSs. It is therefore natural to extend the original method to include the effect of internal volumetric heat sources as follows:

$$\Delta T = \underbrace{\sum_{i=1}^{N_T}(T_{h,i}-T_c)+\sum_{j=1}^{N_F}q''_j H/k_f}_{\text{external wall heat sources}} + \underbrace{\sum_{k=1}^{N_V}q'''_k H^2/k_f}_{\text{internal volumetric heat sources}} \tag{7}$$

where N_T, N_F, and N_V are respectively the number of the ITHS, IFHS and IVHS. Divided by ΔT, above equation becomes

$$\underbrace{\sum_{i=1}^{N_1}\theta_i+\sum_{j=1}^{N_2}\left(-\frac{\partial\theta}{\partial n}\right)_j}_{\text{external}}+\underbrace{\sum_{k=1}^{N_3}S_k}_{\text{internal}}=1 \tag{8}$$

The first two summation terms on the left-hand side of Eq. (8) are respectively the thermal BCs for ITHS and IFHS, and the third term is the source term of the governing Eq. (5) for IVHS. In other words, an individual heat source could be identified by its contribution ratio to the total effect. The contribution ratio from the external surface DHS can be expressed by its thermal BC, but that from the internal volumetric DHS expressed by the source term. For general purpose, the above equation is further written as

$$\sum_i R_{T,i}+\sum_j R_{F,j}+\sum_k R_{V,k}\equiv 1 \tag{9}$$

where R is the contribution ratio and the subscripts T, F, and V represent ITHS, IFHS and IVHS.

By the combined temperature scale method, the different DHSs are clearly identified by their corresponding contribution ratios, and their inherent interactions are physically stated by the correlation, Eq. (9). On the other hand, the method is mathematically complete, which can easily describe the relation between any combination and/or number of DHSs.

2.4. Heat transfer characteristics

To discuss the heat transfer characteristics of a system, the average Nusselt number is usually employed. According to the energy balance across the system, the total energy input from DHSs is equal to the energy released at cold surface, which written in mathematical formula is

$$\sum_i\int_0^{l_i}q''_{T,i}\,ds+\sum_j q''_{F,j}l_j+\sum_k q'''_{V,k}A_k=\int_0^{l_c}q''_{T,c}\,ds \tag{10}$$

Note that the energy transported from the isotherm surface is in an integral form because its heat flux is non-uniform. Non-dimensionalizing equation by multiplying a factor $1/k_f\Delta T$ yields

$$\sum_i\int_0^{l_i/H}\left(-\frac{\partial\theta}{\partial n}\right)ds+\sum_j\frac{q''_{F,j}H}{k_f\Delta T}\frac{l_j}{H}+\sum_k\frac{q'''_{V,k}H^2}{k_f\Delta T}\frac{A_k}{H^2}=\int_0^{l_c/H}\left(-\frac{\partial\theta}{\partial n}\right)ds \tag{11}$$

which written in average Nusselt number form becomes

$$\sum_i\overline{Nu}_{T,i}+\sum_j\overline{Nu}_{F,j}+\sum_k\overline{Nu}_{V,k}=\overline{Nu}_c \tag{12}$$

The average Nusselt number, $\overline{Nu}$, for different types of DHSs are defined as follows:

$$\begin{aligned}\overline{Nu}_T&=\int_0^{l/H}\left(-\frac{\partial\theta}{\partial n}\right)ds=\int_0^{l^*}Nu_T\,ds,\quad\text{for ITHS}\\ \overline{Nu}_F&=\frac{q''H}{k_f\Delta T}\frac{l}{H}=R_F l^*=Nu_F l^*,\quad\text{for IFHS}\\ \overline{Nu}_V&=\frac{q'''H^2}{k_f\Delta T}\frac{A}{H^2}=R_V A^*=Nu_V A^*,\quad\text{for IVHS}\end{aligned} \tag{13}$$

where l^* and A^* are respectively the dimensionless length and area for the external and internal DHSs. It is found that the average Nusselt number of DHS is directly related to the contribution ratio.

In above definitions, the local Nusselt numbers for different DHSs are physically unified, i.e. equal to the dimensionless heat flux, and thus the corresponding average Nusselt numbers represent the heat input from DHSs in dimensionless form. Note that in some literatures [13,15,21,22], the local Nusselt number for the IFHS is defined in terms of surface temperature ($Nu_F=1/\theta$), which can only be used to describe and compare the heat transfer effects for equal heat sources but for different heat sources. On the other hand, there is so far no corresponding parameter to assess the convective heat transfer for the volumetric heat source. The suggested definitions based on energy conservation in the present work are, however, able to make up the deficiencies, and its effectiveness will be demonstrated in the following sections. Note that the idea of using dimensionless heat flux to express the convective heat transfer for the non-uniform temperature surface was first pointed out by Kim and Viskanta in 1984 [23], but unfortunately has never been used.

No doubt that the heat input from an individual heat source would determine its role in the interaction with others. Thus, a more straightforward concept, the thermal strength of a heat source, denoted by Π, is introduced here as follows:

$$\Pi=\overline{Nu} \tag{14}$$

According to expressions in Eqs. (13), one can see that the thermal strength of ITHS is determined by the resultant temperature distribution across the system, which is related not only to the contribution ratio and size of the heat source but also to the Rayleigh number. The thermal strengths of IFHS and IVHS are however only associated with their contribution ratios and sizes, i.e.

$$\Pi = R\omega \tag{15}$$

which can be interpreted as the weighted contribution ratio, and the weight ω is the dimensionless size, either the length l^* for IFHS or the area A^* for IVHS. Therefore, the thermal strength of the ITHS can only be obtained when the temperature field has been solved, but that of the IFHS or IVHS may be known before the numerical solution.

2.5. Boundary conditions

The thermal BCs are: $\theta = 0$ for the cold wall and $\partial\theta/\partial n = 0$ for the adiabatic walls. DHSs are described by their contribution ratios, as shown in Eq. (9).

The velocity BCs for the enclosed walls are all specified by the no-slip condition.

2.6. Numerical procedure

Above governing equations are discretized by using a finite volume method (FVM) on a staggered grid system [24]. The FVM can easily solve the conjugate convection/conduction by using the harmonic mean technique for dealing with the variable diffusion coefficient. In the course of discretization, a third-order deferred correction QUICK scheme [25] and the second-order central difference are, respectively implemented for the convection and diffusion terms. The resulting discretized equations are solved by a line-by-line procedure, combining the tri-diagonal matrix algorithm (TDMA) and the successive over-relaxation iteration. The coupling between velocity and pressure is done by SIMPLE algorithm [24,26]. The convergence of the numerical solution was monitored by checking the energy balance, Eq. (12), across the system.

Non-uniform grid is employed in present study, with denser grids clustering in regions near the DHSs and the enclosed walls. The code used here has been validated in the previous studies [20,26,27]. For each calculation case, a grid independent resolution is obtained.

3. Results and discussion

Based upon foregoing analysis, the solutions of the governing equations are characterized by a set of dimensionless parameters: the Rayleigh number (Ra), the Prandtl number (Pr), and the relative conductivity (k^*), the aspect ratio ($A_r = H/L$), the contribution ratio (R) and size (ω) of DHSs and their separation distance ($W^* = W/H$). In the present study, the values of Pr, k^*, and A_r are kept constant as 0.71, 1.0, and 0.5 respectively, and main attention is focused on the effects of Ra, R, ω, and W^* on the interaction between DHSs for the four calculation cases (Cases 1–4).

Before turning our focus, we first validate the heat transfer analysis suggested in the present work. The test natural convection with DHSs is the configuration as schematically shown in Fig. 1(a), but with only one DHS, either ITHS or IFHS, located center on the floor. According to the energy conservation across the enclosure, the thermal strength (Π) of DHS should be equal

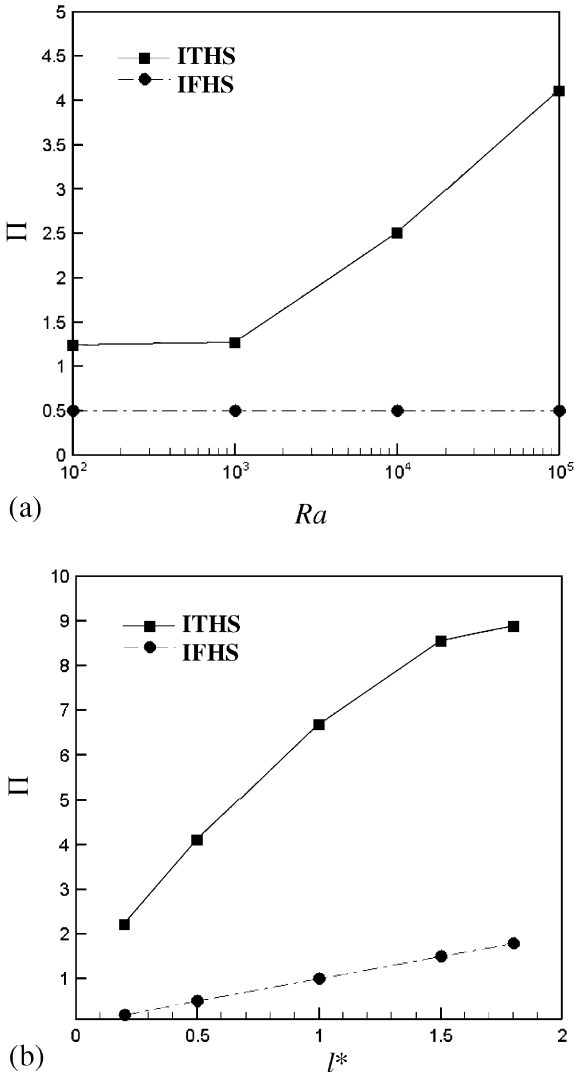

Fig. 2. Influence factors on the thermal strength Π of a discretely heated source: (a) the Rayleigh number Ra and (b) the dimensionless size l^*.

to the average Nusselt number of the isothermal cold wall ($\overline{Nu}_c$), the formulation of the latter being accepted as a standard. As mentioned before, the thermal strength of DHS may be related to three parameters, i.e. $\Pi = f(Ra, R, \omega)$. For there is only one heated source, the contribution ratio is always equal to unity, $R \equiv 1$, and thus its effect on the thermal strength is not shown here, which is however demonstrated in the following interaction analysis. Fig. 2 shows the relation between the thermal strength (Π) and the other two parameters (Ra, ω) for ITHS and IFHS respectively. It is obvious that the thermal strength of ITHS is related not only to Ra but also to R and ω of the heat source, but that of IFHS is only associated with R and ω. The phenomenon is consistent with the analysis before.

3.1. Interaction between two IFHSs on the bottom (Case 1)

3.1.1. Effects of the separation distance between the bottom IFHSs

To consider only the effect of W^*, other parameters are kept constant as $Ra = 10^5$, $R_{F1} = R_{F2} = 0.5$, $l_1^* = l_2^* = 0.25$. The reversed flow patterns and their corresponding thermal structures for $W^* = 0.5$ and $W^* = 1.5$, as shown in Fig. 3, reveal that the buoyancy effects act together for two closer DHSs but act separately for two far DHSs. More detailed information about the effect of the separation distance on the resulting velocity and temperature field is recorded in Fig. 4. The vertical velocity profiles along the horizontal centerline for different separation distances, as plotted in Fig. 4(a), show two different flow patterns: the fluid flows upward at the center and downward along the sidewalls when $W^* < 1$, but the fluid flows upward along the vertical adiabatic sidewalls and downward at the center when $W^* \geqslant 1$. The maximum streamfunction ($|\psi|_m$) monotonously decreases as the distance increases, shown in Fig. 4(b), indicating that the convection is much stronger for the former than that for the latter. The variation of maximum temperature in the flow field (θ_m) in terms of W^* is also shown in Fig. 4(b). Its parabolic profile indicates that θ_m decreases as W^* increases within the region $W^* < 1$, beyond which θ_m increases as W^* increases. This implies that the minimal temperature distribution may occur at a medium distance $W^* = 1$. The minimum temperature is of importance to achieve the optimal heat transfer effect, so one cannot take it for granted that the larger or the smaller the separation distance, the lower the temperature. Therefore, the characteristics of the fluid flow and heat transfer in the enclosure are very sensitive to the separation distance between the IFHSs.

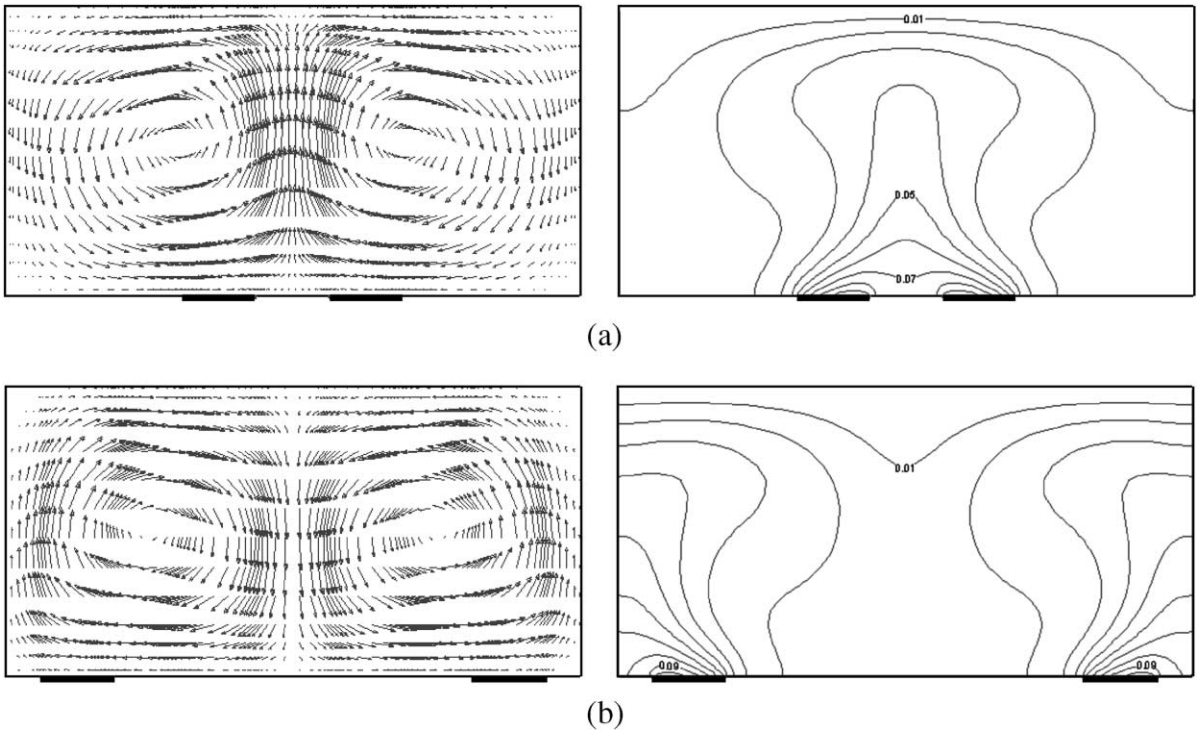

Fig. 3. Velocity vectors and isotherms at different separation distances between two IFHSs for Case 1: (a) $W^* = 0.5$ and (b) $W^* = 1.5$.

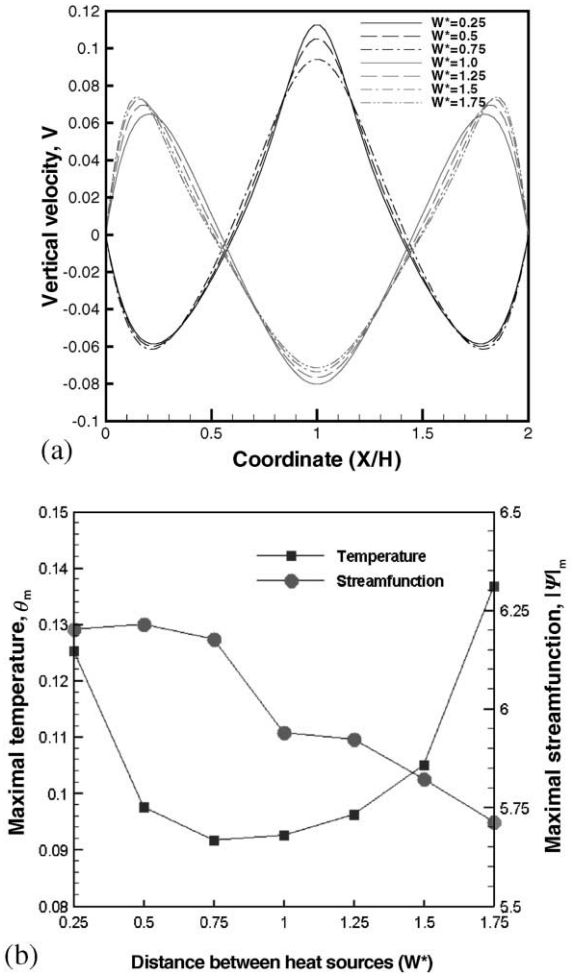

Fig. 4. Effects of the separation distance (W^*) on the resulting velocity and thermal field for Case 1: (a) V–X profile at $Y = 0.5$ and (b) maximal temperature θ_m and maximal streamfunction $|\psi|_m$.

3.1.2. Effects of the thermal strength of the bottom IFHSs

As mentioned before, the thermal strength of DHS is the key factor that determines its influence region, which in the result dominates the fluid flow and heat transfer characteristics. The calculation results have shown that only if the thermal strengths of two IFHSs are equal, their influence regions should be identical, with each occupying half of the enclosure. Fig. 5 shows the velocity vectors and isotherms for two equal IFHSs ($\Pi_1 = \Pi_2$) with one $R_1 = 1/6$, $l_1^* = 0.5$ and the other $R_2 = 5/6$, $l_2^* = 0.1$. However, when $\Pi_1 \neq \Pi_2$, the interaction between two IFHSs shows different manners in three aspects. First, when two IFHSs are separated at a smaller distance, as shown in Fig. 6(a) at $W^* = 0.5$, the upward plume splits the enclosure into two parts, but moves closer to the stronger heat source side, above which a steeper temperature gradient appears in the isotherms. Second, when two IFHSs are separated at a medium distance, shown in Fig. 6(b) at $W^* = 1.0$, it is surprising to find that the flow is merged into single circulating cell across the enclosure. In this situation, the fluid is heated in advance by the weaker IFHS before it reaches the stronger IFHS, and thus heat is a cumulated above the stronger IFHS, as seen in isotherms that the temperature is horizontally stratified. The heat and fluid flow patterns are very similar to those occurring in a vertical enclosure [5]. Third, when the distance expands further as shown in Fig. 6(c) at $W^* = 1.5$, two circulating cells appear in the fluid flow again, but now the flows are induced upward by buoyancy along the vertical sidewalls. Meanwhile the two cells are not identical in size, the flow set up by the stronger IFHS occupying a larger space than that by the weaker one.

3.2. Interaction between the bottom ITHS and two IVHSs (Case 2)

For the sake of simplicity, the dimensionless sizes of both ITHS and IVHSs are kept invariant as $l^* = 2.0$,

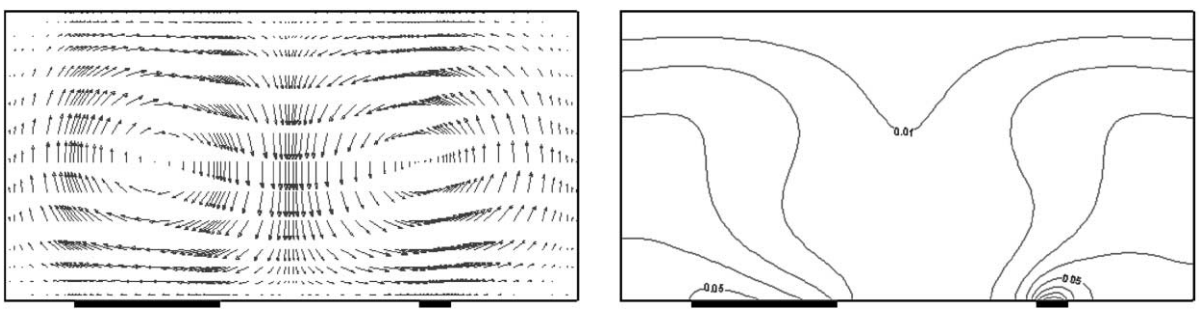

Fig. 5. Velocity vectors and isotherms for two equal IFHSs at separation distance $W^* = 1.0$ for Case 1: $\Pi_1 = R_1\omega_1 = 1/6 \times 0.5 = 1/12$, $\Pi_2 = R_2\omega_2 = 5/6 \times 0.1 = 1/12$.

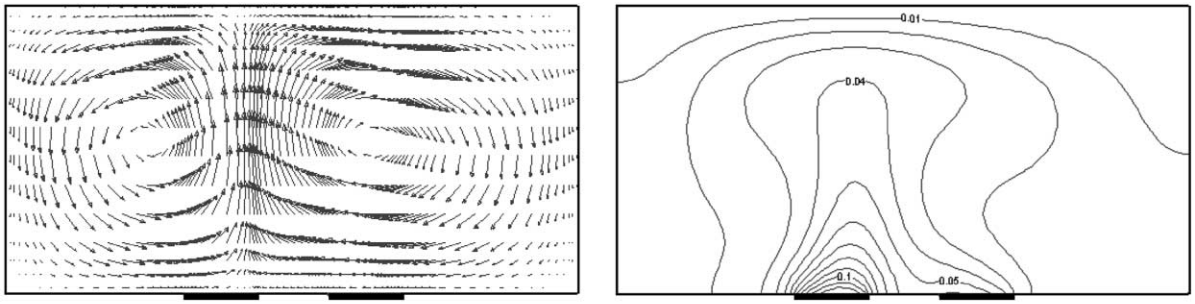

(a) $\Pi_{F1} = R_1 \cdot \omega_1 = 0.7 \times 0.25 > \Pi_{F2} = R_2 \cdot \omega_2 = 0.3 \times 0.25$

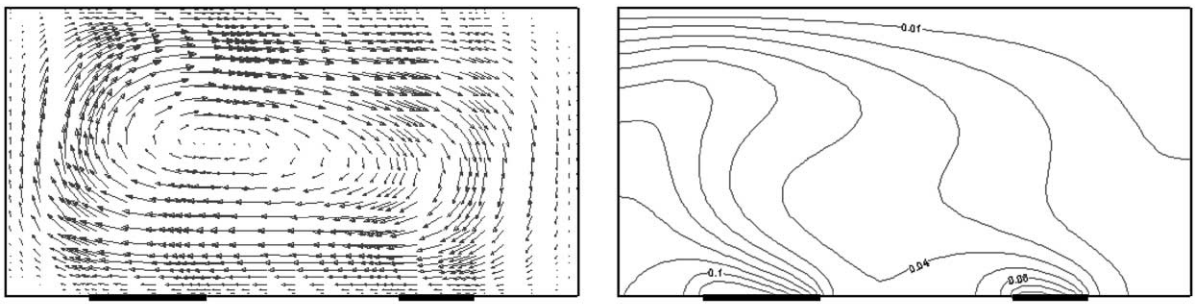

(b) $\Pi_{F1} = R_1 \cdot \omega_1 = 0.5 \times 0.4 > \Pi_{F2} = R_2 \cdot \omega_2 = 0.5 \times 0.2$

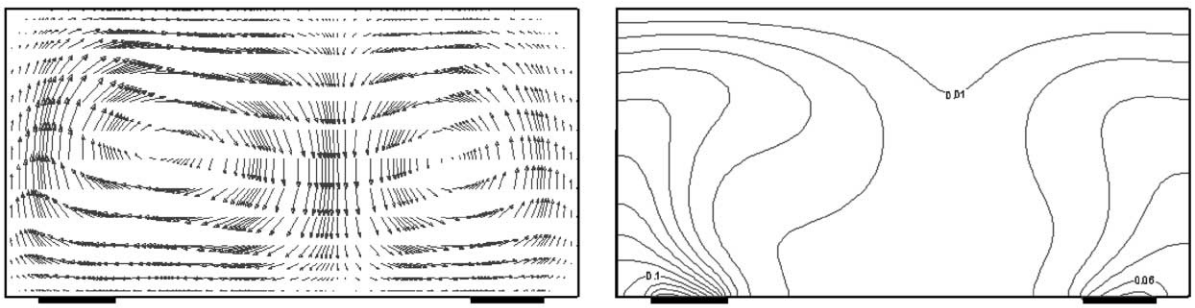

(c) $\Pi_{F1} = R_1 \cdot \omega_1 = 0.7 \times 0.25 > \Pi_{F2} = R_2 \cdot \omega_2 = 0.3 \times 0.25$

Fig. 6. Velocity vectors and isotherms for two non-equal IFHSs at different separation distance W^* for Case 1: (a) $W^* = 0.5$; (b) $W^* = 1.0$; (c) $W^* = 1.5$.

$A^* = 0.5 \times 0.5$, and the separation distance between two IVHSs are fixed at $W^* = 1.0$. Main attention is focused on the effects of the contribution ratio R and the Rayleigh number Ra.

3.2.1. Bottom ITHS and two equal IVHSs

3.2.1.1. Effects of the contribution ratio R. Fig. 7 shows the streamlines and isotherms at different contribution ratios between DHSs for $Ra = 10^5$. It is clear that the interaction between the bottom ITHS and two equal IVHSs is very complicated and changes with the contribution ratios. To begin with, shown in Fig. 7(a) is that the bottom ITHS is the only heat contribution across the enclosure with two inner conducting bodies without heat-generating rate, i.e. $R_T = 1.0$, $R_{V1} = R_{V2} = 0$. The convection is now very strong, $|\psi|_m = 13.7$, with two symmetrically circulating cells surrounding the conducting bodies. The strong convection effect is more pronounced in the isotherms where the thermal boundary layers are fully developed along the bottom hot and top cold walls respectively, and also the isotherms pass through the conducting bodies from the inner to outside. The main structures of fluid flow and heat transfer are maintained over a wide range, as shown in Fig. 7(b)

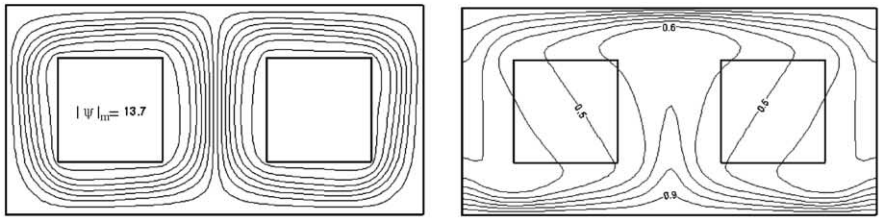

(a) R_T=1.0, R_{V1}= R_{V2}=0.0

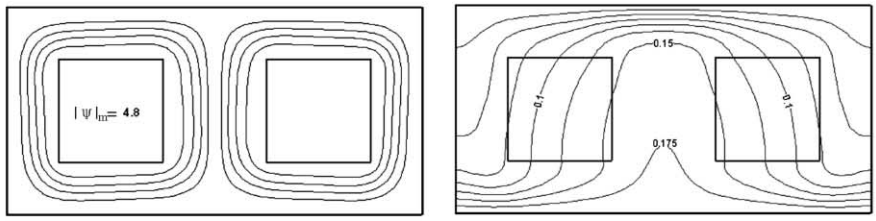

(b) R_T=0.2, R_{V1}= R_{V2}=0.4

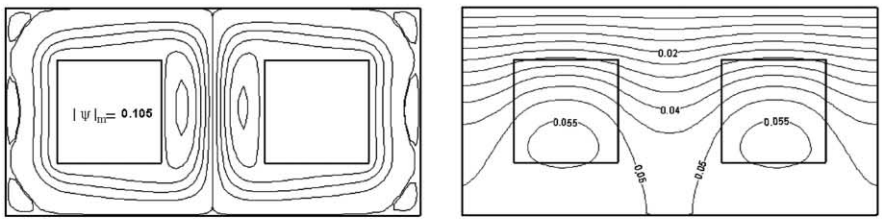

(c) R_T=0.05, R_{V1}= R_{V2}=0.475

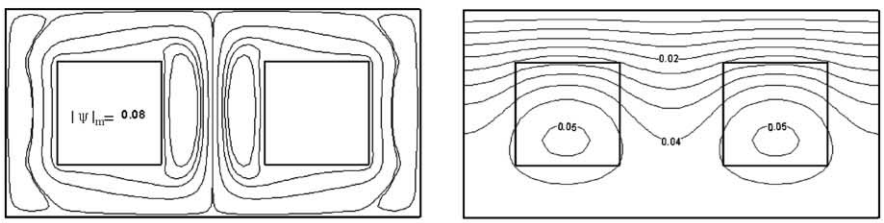

(d) R_T=0.04, R_{V1}= R_{V2}=0.48

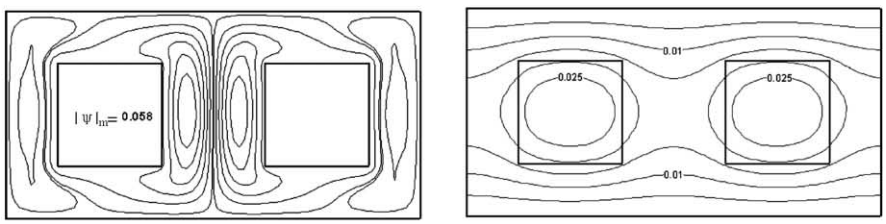

(e) R_T=0.0, R_{V1}= R_{V2}=0. 5

Fig. 7. Interaction between the bottom ITHS and two equal IVHSs for Case 2 at $Ra = 10^5$.

where R_T is decreased to 0.2. However, the convection is much weakened as the strength of ITHS decreases, and accordingly the thermal boundary layers are gradually degenerated.

When the contribution ratio of the bottom ITHS is low enough, or equivalently the strengths of IVHSs are very strong, the fluid flow and heat transfer structures would be very different. Shown in Fig. 7(c) is the streamlines and isotherms for $R_T = 0.05$ and $R_{V1} = R_{V2} = 0.475$. The convection is currently very weak, $|\psi|_m = 0.105$, and thus the heat transfer is mainly dominated by conduction. Streamlines show that the flow structure is very complicated: besides the main cells surrounding the IVHSs, secondary flows have developed in the gap between the main flows and the heat source surfaces, and even tertiary flows begin to form at the top, center, and bottom corners along the vertical sidewalls. The denser parallel-like isotherms in the upper region indicate that the most amount of the heat of the system is released by conducting through the top cold wall. While rare isotherms in the lower region indicate that there is a very small amount of heat that is reversely transferred from IVHSs to ITHS through the fluid (note that for bottom ITHS, its surface temperature or BC is equal to its contribution ratio, 0.05). Isotherms also show that the maximum temperature appears near the bottom side of the IVHSs. When the contribution ratio of the bottom ITHS decreases further, as shown in Fig. 7(d) where $R_T = 0.04$ and $R_{V1} = R_{V2} = 0.48$, the convection is weakened further, however the secondary flows become stronger and the tertiary flows gradually develop. Isotherms indicate that the heat transferred from IVHSs to the bottom ITHS increases for the temperature gradient in the lower channel has been exaggerated, and that the maximum temperature moves towards inside IVHSs. When the contribution ratio from the bottom ITHS vanishes, the heat transfer across the enclosure is fully contributed from the IVHSs. The bottom wall is then turned into a cold surface same as the top wall. The fluid flow and heat transfer structure are basically symmetric along the horizontal centerline, as seen by the streamlines and isotherms in Fig. 7(e). At this time, the primary, secondary, and tertiary cells are all fully developed, on the other hand, the heat transferred from the bottom wall is equal to that from the top cold wall, and the maximum temperature is located in the center of the IVHSs.

The variations of the maximum streamfunction ($|\psi|_m$) and the average Nusselt numbers of both bottom ITHS and top cold wall ($\overline{Nu}_T$, $\overline{Nu}_c$) in terms of R_T at $Ra = 10^5$ are shown in Fig. 8. It is found that the whole effect of R_T can be divided into two regimes: a conduction regime at $R_T \in (0, 0.05)$ and a convection or laminar regime at $R_T \in (0.05, 1)$, with the transition point at $R_T = 0.05$. The fluid flow and heat transfer characteristics in the two regimes are quite different. In the conduction regime the convection is very weak and hence heat transfer is mainly dominated by conduction, and therefore the convection and heat transfer are not sensitive to R_T. In the convection regime, convection is the overwhelming behavior and thus the convection and heat transfer are enhanced rapidly as R_T increases. On the other hand, the conduction regime is dominated by two IVHSs, but the convection regime is dominated by the bottom ITHS. In the figure, the difference of the average Nusselt numbers between the bottom ITHS and the top cold wall is the total average Nusselt number of the IVHSs, i.e. $\overline{Nu}_{V,1+2} = \overline{Nu}_c - \overline{Nu}_T$, which diminishes as R_T increases or R_V decreases, for the relation $\overline{Nu}_V = R_V A^*$ holds.

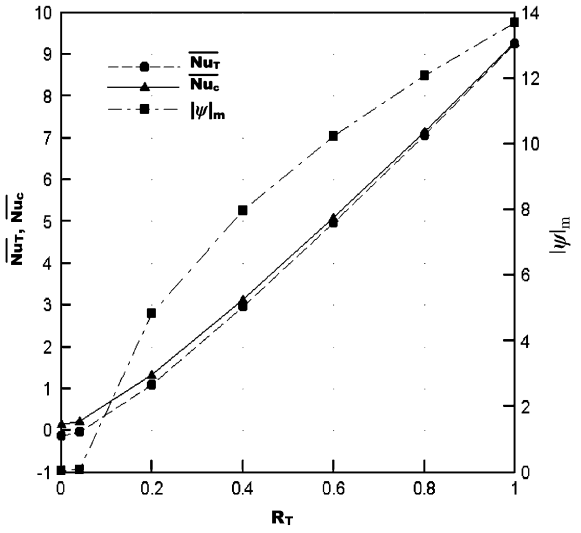

Fig. 8. Variations of the maximal streamfunction ($|\psi|_m$) and the average Nusselt number ($\overline{Nu}$) in terms of the contribution ratio of the bottom ITHS (R_T) at $Ra = 10^5$.

3.2.1.2. Effects of the Rayleigh number Ra. For the thermal strength of ITHS is much related to *Ra*, the interaction between the bottom ITHS and two IVHSs should be influenced by the parameter. Shown in Fig. 9 are variations of the streamfunction ($|\psi|_m$) and the average Nusselt numbers ($\overline{Nu}_T$, $\overline{Nu}_V$, and $\overline{Nu}_c$) in terms of R_T at $Ra = 10^4$. It is found that the *Ra* decreasing has delay the transition from conduction to convection, from the previous $R_T = 0.05$ at $Ra = 10^5$ to the current $R_T = 0.6$. This is due to the fact that the thermal strength of the ITHS decreases with *Ra*, and accordingly both the average Nusselt number and the convection decrease. A similar flow and thermal patterns were observed in the conduction and convection regimes as seen in $Ra = 10^5$.

3.2.2. Bottom ITHS and two non-equal IVHSs

As mentioned above, the heat and fluid flow structures are dominated by the bottom ITHS in the convection regime but by two IVHSs in the conduction regime. Therefore, the inequality between the two

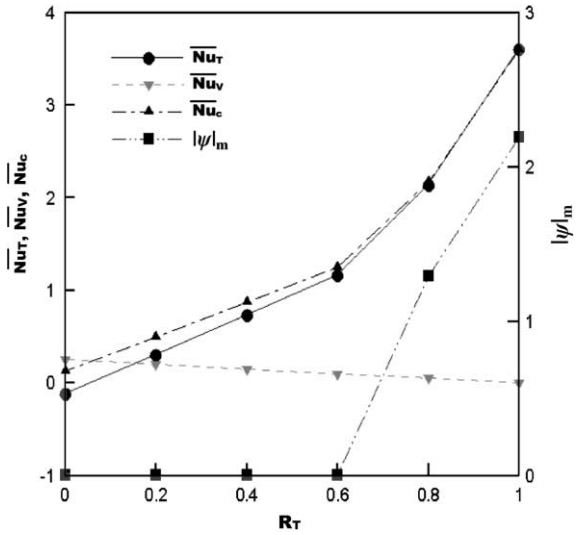

Fig. 9. Variations of the maximal streamfunction ($|\psi|_m$) and the average Nusselt number ($\overline{Nu}$) in terms of the contribution ratio of the bottom ITHS (R_T) at $Ra = 10^4$.

IVHSs would not have much influence on the heat and fluid flow structures in the convection regime, but it does in the conduction regime. Fig. 10 shows the interaction between the bottom ITHS and two unequal IVHSs at $Ra = 10^5$. It is observed that in the convection regime $R_T = 0.2 \in (0.05, 1.0)$, the inequality between the two IVHSs, as set by $R_{V1} = 0.6$ and $R_{V2} = 0.2$, has little effect on the resulting streamlines and isotherms, as compared to the corresponding equality case of Fig. 7(b). However in the conduction regime $R_T = 0.04 \in (0.0, 0.05)$, the inequality between the two IVHSs has greatly effect on the resulting fluid flow and hear transfer structures. Streamlines indicate that the weaker IVHS is fully located in the wake induced by the stronger IVHS, and isotherms show that the heat is accumulated by the fluid flow.

3.3. Interaction between the bottom IFHS and two IVHSs (Case 3)

Now change the bottom ITHS of Case 2 into an IFHS, so that we can investigate the interaction between the bottom IFHS and two IVHSs.

3.3.1. Effects of the contribution ratio R

Fig. 11 presents the interaction between the bottom IFHS and two IVHSs by means of the isotherms obtained at different contribution ratios of the DHSs for $Ra = 10^5$. Seen from the isotherms, we can expect that only if the bottom IFHS exists ($R_F > 0$), the resulting fluid flows are always composed of two symmetric cells which driven upward by buoyancy in the center region, surrounding two IVHSs. However the convection is decreased as the contribution ratio of the bottom IFHS decreases, because the isotherms are getting smoother

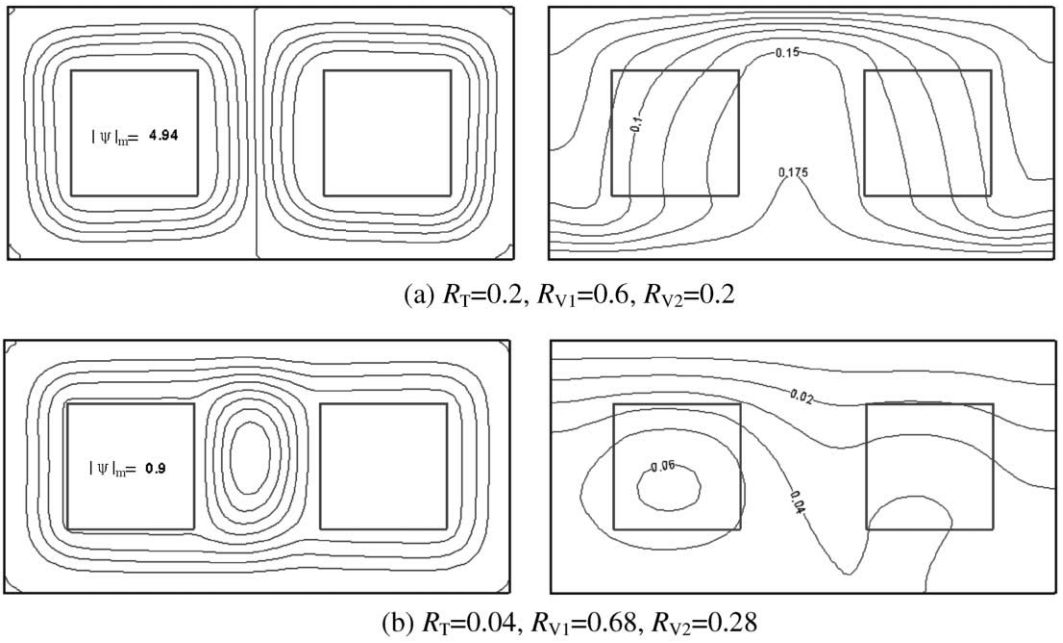

Fig. 10. Interaction between the bottom ITHS and two non-equal IVHSs for Case 2 at $Ra = 10^5$.

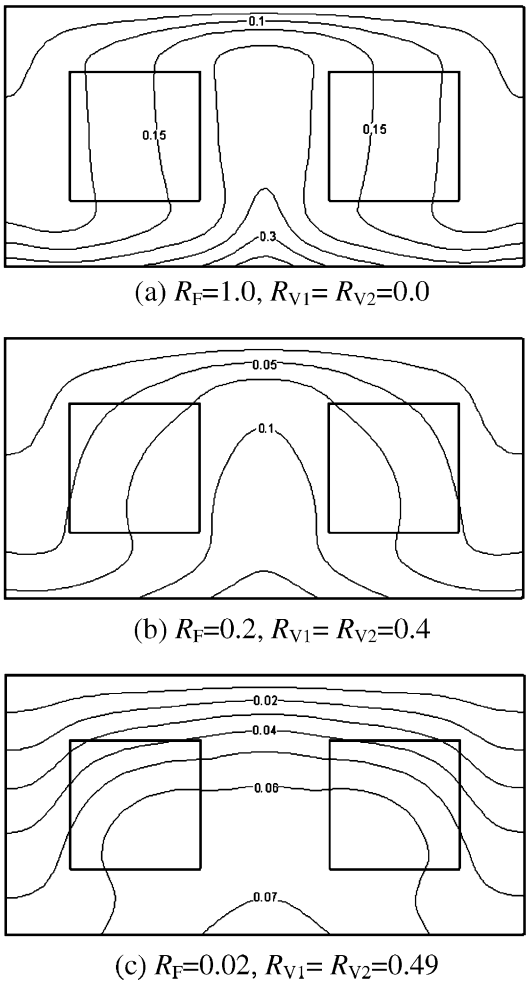

Fig. 11. Interaction between the bottom IFHS and two equal IVHSs for Case 3 at $Ra = 10^5$.

and smoother. The variations of the maximum streamfunction and the average Nusselt numbers in terms of R_F are shown in Fig. 12. It is clear that the full procedure lies in the convection regime, and thus the inequality between the two IVHSs would not have much influence on the resulting the flow and thermal patterns. The average Nusselt numbers of both the bottom IFHS and two IVHSs linearly change with the contribution ratio R_F with the former linearly increasing with R_F but the latter decreasing with R_F, as indicated by $\overline{Nu} = R\omega$. The total heat transfer across the system is correlated by $\overline{Nu}_c = \overline{Nu}_F + \overline{Nu}_V$.

3.3.2. Effects of the Rayleigh number Ra

Fig. 12 also shows the results at $Ra = 10^4$. For the thermal strengths of both IFHS and IVHSs are not related to Ra, the heat transfer characteristics across the

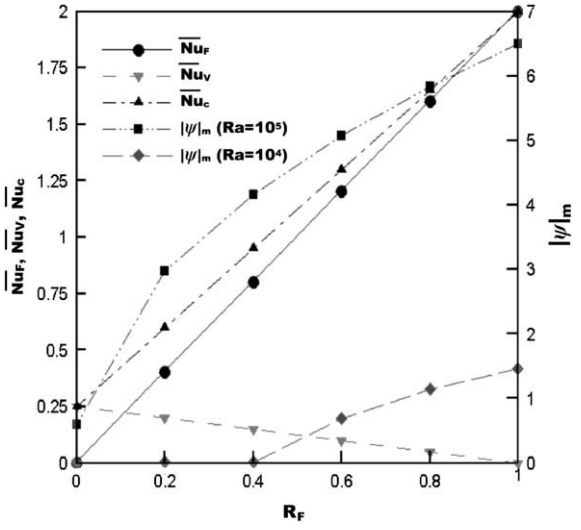

Fig. 12. Variations of the maximal streamfunction ($|\psi|_m$) and the average Nusselt number ($\overline{Nu}$) in terms of the contribution ratio of the bottom IFHS (R_F) at both $Ra = 10^5$ and 10^4.

enclosure are not affected, and thus identical to the case $Ra = 10^5$. But the fluid flow structures are different. The variation of $|\psi|_m$ in terms of R_F is now again divided into two parts: conduction regime, $R_F \in (0, 0.4)$, and convection regime, $R_F \in (0.4, 1.0)$.

3.4. Interaction between two IVHSs (Case 4)

If the heat flux from the bottom IFHS of Case 3 vanishes, the problem turns into the interaction between two IVHSs. This case is very similar to the interaction between two bottom IFHSs of Case 1.

3.4.1. Effects of the separation distance between the IVHSs

The separation distance (W^*) between the IVHSs also has an important effect on the resulting heat and fluid flow structures, as shown in Fig. 13. At first, when the two sources are located very close, $W^* = 0.6$, the flow pattern consists of two main symmetric cells surrounding IVHSs induced by the buoyancy effect in the center region, and two secondary cells formed near the outward ends of the two IVHSs. Influenced by the flow field, the steep temperature gradient appears in the center region, with the maximum temperature ($\theta_m = 0.07$) located in the inward bottom corners of the IVHSs. When W^* increases to 0.8, the main circulating flows around IVHSs strengthen, which causes the secondary flows diminishes. The isotherms show that the maximum temperature is reduced to $\theta_m = 0.056$ and moves outward. However, when W^* increases to a me-

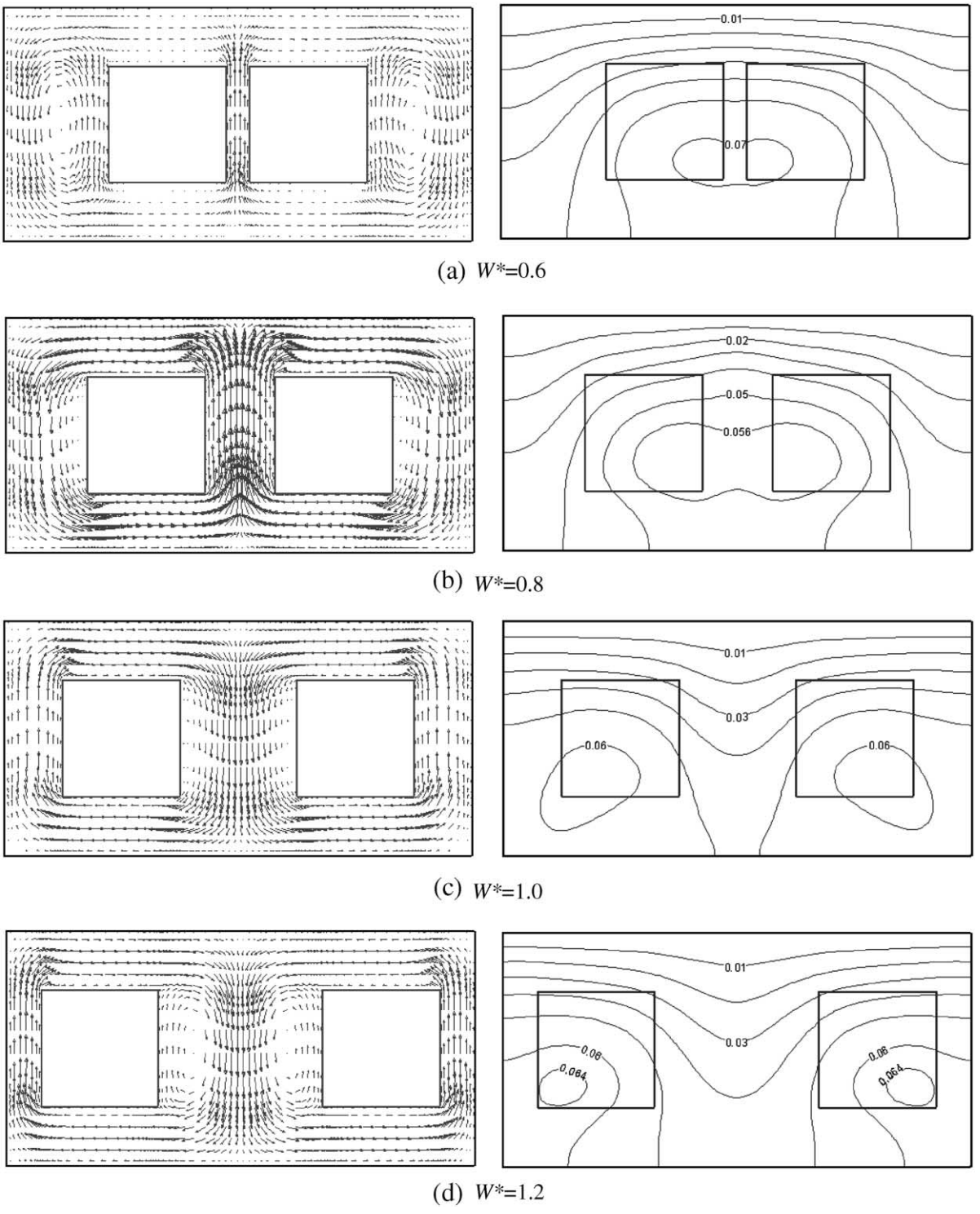

Fig. 13. Velocity vectors and isotherms at different distance (W^*) between two equal IVHSs for Case 4 at $Ra = 10^5$.

dium size, 1.0, the heat and fluid flow structures are quite different. Velocity vectors show that the fluid is first driven upward by the buoyancy along the sidewalls, then turns downward in the center region, and forms

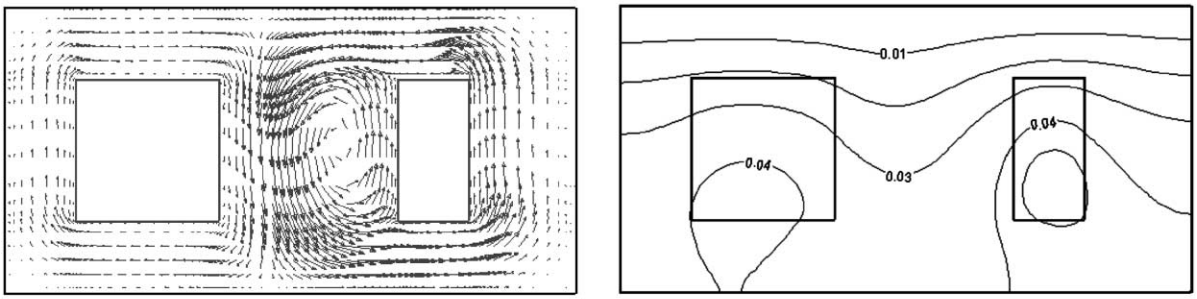

(a) two IVHSs with equal thermal strength

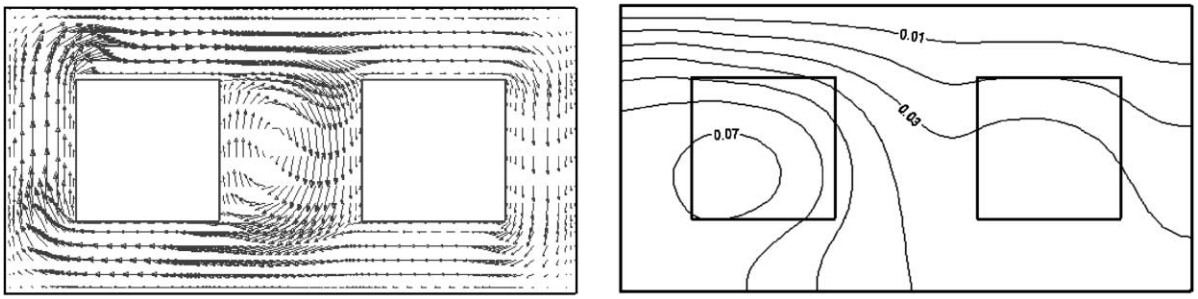

(b) two IVHSs with unequal thermal strength

Fig. 14. Velocity vectors and isotherms for two IVHSs with (a) unequal and (b) equal strengths.

two symmetric cells surrounding the IVHSs. Accordingly, the isotherms reveal that the steep temperature gradient appears along the sidewalls, and thus the maximum temperature $\theta_m = 0.06$ lies in outward bottom corners of the IVHSs. But it is interesting to find that the maximum temperature begins to increase. Finally, when the separation distance increases further, $W^* = 1.2$, velocity vectors show that two secondary cells appear near the inward ends of the IVHSs. The isotherms reveal that the maximum temperature $\theta_m = 0.064$ continues increasing and moves outward further. It is demonstrated that the characteristics of the fluid flow and heat transfer in the enclosure are also sensitive to the separation distance between the IVHSs, and the above trend about the variations of the flow directions and the maximum temperature distribution closely resemble the pattern observed in the Case 1.

3.4.2. Effects of the thermal strength of the IVHSs

Fig. 14 shows two IVHSs separated at $W^* = 1.0$ with equal and non-equal thermal strengths. It is found that when two IVHSs are of equal thermal strengths, their influence regions are nearly the same size, with each occupying half of the enclosure. But when their thermal strengths are not identical, the weak one would be always located in the wakes of the strong one, and thus heat is accumulated toward the strong IVHS. The effect of thermal strength on the interaction between DHSs is also very similar to the Case 1.

4. Conclusions

Two-dimensional, steady, laminar natural convection in horizontal enclosures induced by multiple wall and volumetric DHSs has been numerically studied. A combined temperature scale method and a unified heat transfer characteristics analysis have been suggested to describe the heat sources of different type, size and strength. The method is found to be general and efficient to evaluate the interactions between DHSs and their effects on the overall heat and fluid flow structures.

The interactions between both the two IFHSs on the floor and the two IVHSs have revealed that: (1) There are two different flow and thermal patterns according to the separation distance W^*. When $W^* < 1$, the two DHSs act together in the center region, which causes the flow being induced upward in the center region, and the maximum temperature decreases as the W^* increases.

When $W^* \geqslant 1$, however, the two DHSs act separately, which causes the downward flow in the center region, and the maximum temperature increases with W^*. (2) When the thermal strengths of the two DHSs are identical, irrespective of their different contribution ratios and sizes, their influence regions are basically the same, i.e. half of the enclosure. But when their thermal strengths are not equal, the fluid flow is mainly determined by the stronger DHS.

The interactions between the bottom ITHS or IFHS and the two IVHSs have shown that according to the contribution ratios of DHSs, the flow structures can be divided into two regimes, i.e. the conduction regime and the convection regime. The conduction regime is mainly determined by the two IVHSs, and the flow structure is very complex which is composed of main, secondary, and tertiary flows. However, the convection regime is ruled by the bottom heat source, and the flow structure simply consists of two main cells circulating around the IVHSs. Accordingly, the inequality between the two IVHSs would have much influence on the flow structure in the conduction regime, but that would not work in the convection regime.

References

[1] B. Gebhart, Y. Yaluria, R.L. Mahajan, B. Sammakia, Buoyancy-Induced Flows and Transport, Hemisphere, Washington, DC, 1988.

[2] F.P. Incropera, Convection heat transfer in electronic equipment cooling, ASME J. Heat Transfer 110 (1988) 1097–1109.

[3] S. Ostrach, Natural convection in enclosures, ASME J. Heat Transfer 110 (1988) 1175–1190.

[4] E.M. Sparrow, M. Faghri, Natural convection heat transfer from the upper plate of a collinear, separated pair of vertical plates, ASME J. Heat Transfer 102 (1980) 623–629.

[5] Y. Jaluria, Buoyancy-induced flow due to isolated thermal sources on a vertical surface, ASME J. Heat Transfer 104 (1982) 223–227.

[6] Y. Jaluria, Interaction of natural convection wakes arising from thermal sources on a vertical surface, ASME J. Heat Transfer 107 (1985) 883–892.

[7] M. Afrid, A. Zebib, Natural convection air cooling of heated components mounted on a vertical wall, Numer. Heat Transfer, Part A 15 (1989) 243–259.

[8] H.Y. Wang, F. Penot, J.B. Sauliner, Numerical study of a buoyancy-induced flow along a vertical plate with discretely heated integrated circuit packages, Int. J. Heat Mass Transfer 40 (1997) 1509–1520.

[9] M. Keyhani, V. Prasad, R. Cox, An experiment study of natural convection in a vertical cavity with discrete heat source, ASME J. Heat Transfer 110 (1988) 616–624.

[10] M.L. Chadwick, B.W. Webb, H.S. Heaton, Natural convection from two-dimensional discrete heat sources in a rectangular enclosure, Int. J. Heat Mass Transfer 34 (1991) 1679–1693.

[11] C.J. Ho, J.Y. Chang, A study of natural convection heat transfer in a vertical rectangular enclosure with two-dimensional discrete heating: effect of aspect ratio, Int. J. Heat Mass Transfer 37 (1994) 917–925.

[12] Y. Ju, Z. Chen, Numerical simulation of natural convection in an enclosure with discrete protruding heaters, Numer. Heat Transfer, Part A 30 (1996) 207–218.

[13] S.K.W. Tou, C.P. Tso, X. Zhang, 3-D numerical analysis of natural convective liquid cooling of a 3×3 heater array in rectangular enclosures, Int. J. Heat Mass Transfer 42 (1999) 3231–3244.

[14] Y.S. Sun, A.F. Emery, Effects of wall conduction, internal heat sources and internal baffle on natural convection heat transfer in a rectangular enclosure, Int. J. Heat Mass Transfer 40 (1997) 915–929.

[15] J.Y. Oh, M.Y. Ha, K.C. Kim, Numerical study of heat transfer and flow of natural convection in an enclosure with a heat-generating conducting body, Numer. Heat Transfer, Part A 31 (1997) 289–303.

[16] M.Y. Ha, M.J. Jung, Y.S. Kim, A numerical study on transient heat transfer and fluid flow of natural convection in an enclosure with a heat-generating conducting body, Numer. Heat Transfer, Part A 35 (1999) 415–434.

[17] M.Y. Ha, M.J. Jung, A numerical study on three-dimensional conjugate heat transfer of natural convection and conduction in a differentially heated cubic enclosure with a heat-generating cubic conducting body, Int. J. Heat Mass Transfer 43 (2000) 4229–4248.

[18] J.J.S. Chu, S.W. Churchill, C.V.S. Patterson, The effects of heater size, location, aspect ratio, and boundary conditions on two-dimensional, laminar, natural convection in rectangular channels, ASME J. Heat Transfer 98 (1976) 194–201.

[19] A.A.M. Sezai, Natural convection from a discrete heat source on the bottom of a horizontal enclosure, Int. J. Heat Mass Transfer 43 (2000) 2257–2266.

[20] Q.-H. Deng, G.-F. Tang, Y. Li, A combined temperature scale for analyzing natural convection in rectangular enclosures with discrete wall heat sources, Int. J. Heat Mass Transfer 45 (2002) 3437–3446.

[21] M.M. Ganzarolli, L.F. Milanez, Natural convection in rectangular enclosures heated from below and symmetrically cooled from the sides, Int. J. Heat Mass Transfer 38 (1995) 1063–1073.

[22] T.J. Heindel, S. Ramadhyani, F.P. Incropera, Laminar natural convection in a discretely heated cavity: I—assessment of three-dimensional effects, ASME J. Heat Transfer 117 (1995) 902–909.

[23] D.M. Kim, R. Viskanta, Study of the effects of wall conductance on natural convection in a differentially oriented square cavities, J. Fluid Mech. 144 (1984) 153–176.

[24] S.V. Patankar, Numerical Heat Transfer and Fluid Flow, Hemisphere, Washington, DC, 1980.

[25] T. Hayase, J.A.C. Humphrey, R. Greif, A consistently formulated QUICK scheme for fast and stable convergence using finite-volume iterative calculation procedures, J. Comput. Phys. 98 (1992) 108–118.

[26] Q.-H. Deng, G.-F. Tang, Special treatment of pressure-correction based on continuity conservation in pressure-based algorithm, Numer. Heat Transfer, Part B 42 (2002) 1–20.

[27] Q.-H. Deng, G.-F. Tang, Numerical visualization of mass and heat transport for conjugate natural convection/heat conduction by streamline and heatline, Int. J. Heat Mass Transfer 45 (2002) 2373–2385.